Journal of Geophysical Research: Atmospheres

RESEARCH ARTICLE
10.1029/2017JD027391

# Different Global Precipitation Responses to Solar, Volcanic, and Greenhouse Gas Forcings

**Fei Liu[1], Tianlang Zhao[1], Bin Wang[2], Jian Liu[3], and Wubian Luo[1]**

[1]Earth System Modeling Center and Climate Dynamics Research Center, Nanjing University of Information Science and Technology, Nanjing, China, [2]Department of Atmospheric Sciences and Atmosphere-Ocean Research Center, University of Hawaii at Manoa, Honolulu, HI, USA, [3]Key Laboratory of Virtual Geographic Environment of Ministry of Education, School of Geography Science, Nanjing Normal University, Nanjing, China

**Key Points:**
- Solar, volcanic, and GHG forcings can excite different low-frequency variabilities of global mean temperature and precipitation
- There is no Arctic amplification of temperature decrease under the volcanic forcing-induced global cooling
- Volcanic eruptions tend to reduce precipitation rather than stop the Arctic amplification under the GHG-induced global warming

**Correspondence to:**
F. Liu,
liuf@nuist.edu.cn

**Citation:**
Liu, F., Zhao, T., Wang, B., Liu, J., & Luo, W. (2018). Different global precipitation responses to solar, volcanic, and greenhouse gas forcings. *Journal of Geophysical Research: Atmospheres*, *123*. https://doi.org/10.1029/2017JD027391

Received 2 JUL 2017
Accepted 2 APR 2018
Accepted article online 12 APR 2018

**Abstract** Understanding climate change caused by different external forcings is an urgent need for crisis management and sustainable economic development. It remains unclear how differently global precipitation changes in response to global temperature variations induced by the change of individual solar, volcanic, or greenhouse gas (GHG) forcings. We address this issue by performing three last millennium simulations under each of these individual forcings with the Community Earth System Model version 1.0. The results show that all three forcings can excite strong low-frequency variations that are longer than one decade, that is, global warming under strong solar radiation or high GHG concentration and global cooling under frequent volcanic eruptions. For a given global temperature change, the global precipitation change under volcanic forcing is larger than that under solar and GHG forcings. The reason is that the volcanic forcing induces the strongest solar irradiance change in the wet tropics. Among the three forcings we examined, the GHG forcing excites the strongest high-latitude warming, especially the Arctic amplification of global warming. There is no Arctic amplification of temperature decrease under the volcanic forcing-induced global cooling. The volcanic forcing weakens the Intertropical Convergence Zone and reduces precipitation. The results suggest that while volcanic eruptions can reduce precipitation, they do not mitigate the Arctic amplification of temperature increase under the GHG-induced warming. The underlying mechanisms for these different climate responses are also discussed.

## 1. Introduction

How will global precipitation change if greenhouse gas (GHG) concentration continues to increase but solar radiation decreases or volcanic eruptions are active? Answering this question is important for safeguarding water resources under global warming. Using stratospheric aerosol modification to mitigate global warming, there is a potential risk of slowing down the global hydrological cycle and reducing water availability, as has already been noted by the Geoengineering Model Intercomparison Project (Jones et al., 2013; Niemeier et al., 2013; Niemeier & Tilmes, 2017; Robock, 2016; Robock et al., 2008). Thus, it is urgent for us to understand the global climate responses to individual external forcings.

The global hydrological cycle has been shown to be more sensitive to shortwave forcing, that is, solar forcing (Andrews et al., 2010; Cao et al., 2012), volcanic forcing (Iles et al., 2013), or combined solar and volcanic forcing (Liu et al., 2013; Wu et al., 2013), than to GHG forcing. To understand global hydrological sensitivity to different individual forcings, the perturbation energy budget of the troposphere is often analyzed (Allen & Ingram, 2002; Kvalevåg et al., 2013; Mitchell et al., 1987; O'Gorman et al., 2012; Wu et al., 2013). The change of the hydrological cycle intensity is controlled not only by the availability of moisture but also by the availability of energy (Mitchell et al., 1987). Based on the Clausius-Clapeyron relation, the saturation vapor pressure should increase by about 7% for each 1°C increase in temperature, while simulations show a very small increase on the order of 2%/°C in global precipitation under the GHG-induced global warming. The reason is the stabilization of the atmosphere, because the GHGs warm the entire troposphere (Held & Soden, 2006). Although the hydrological cycle is found to be more sensitive to natural solar or volcanic forcing than to anthropogenic GHG forcing, quantitative understanding of the sensitivity to these individual solar, volcanic, and GHG forcings remains incomplete, since the natural solar and volcanic forcings are not fully separated in these works. The main target of this work is to fill this gap.

Studying the spatial distributions of these responses to different forcings is also necessary. Under global warming, global precipitation is generally increased in the tropics and high latitudes, while it is decreased in

the subtropics (Meehl et al., 2007). In a last millennium simulation, Liu et al. (2013) found that the hydrological cycle is strong and is tied to La Niña-like sea surface temperature (SST) gradients under the warming induced by increased solar radiation, while it is weak and is tied to El Niño-like SST gradients under the GHG-induced global warming. This reconciles the controversial findings in the paleorecords and modern modeling results; that is, palaeoproxy evidence indicates that a La Niña-like SST pattern occurred in the past periods when the Earth warmed as a result of increased solar radiation (Cobb et al., 2003; Liu et al., 2015; Mann et al., 2005, 2009), whereas in most model projections of future greenhouse warming, this gradient weakens or an El Niño-like SST pattern occurs (Held & Soden, 2006; Meehl & Washington, 1996; Vecchi et al., 2006).

In addition to the aforementioned zonal distribution of temperature change, that is, the El Niño- or La Niña-like SST change, the meridional distribution of global temperature change also has a significant effect on global precipitation change. Arctic amplification in terms of temperature increase has been found in paleorecords, as well in historical observations and climate model experiments (Barron, 1983; Bekryaev et al., 2010; Chapman & Walsh, 1993; Dahljensen et al., 1998; Holland & Bitz, 2003; Manabe & Wetherald, 1975). Diminishing sea ice has been discovered to play a leading role in the recent Arctic temperature amplification (Screen & Simmonds, 2010; Serreze & Francis, 2006). Arctic amplification is also attributed to two other feedbacks: the Planck feedback and the lapse-rate feedback (Pithan & Mauritsen, 2014; Zhang & Li, 2014). The Planck feedback, that is, a larger temperature increase is caused at colder background temperatures for a given radiation increase (Planck, 1901), mainly works to warm the cold polar region, resulting in a vertically uniform warming from the surface to the troposphere. The lapse rate feedback acts to excite greater warming in the upper troposphere than at the surface in the tropics through diabatic heating, resulting in stronger Arctic than tropical surface warming (Bintanja et al., 2012; Manabe & Wetherald, 1975). Since the high-latitude region has much less moisture than the tropical region, different meridional distributions of temperature increase and the associated circulation change should cause different changes of the total moisture convergence and precipitation. Global warming due to different Arctic amplifications induced by changes of these external forcings may cause different precipitation responses. It is interesting to explore how these external forcings affect the meridional distributions of global surface temperature and precipitation.

Recent studies revealed that volcanic eruptions at different latitudes have asymmetric effects on the climate system (Colose et al., 2016; Haywood et al., 2013; Liu et al., 2016; Pausata et al., 2015; Stevenson et al., 2016). Volcanic forcing can influence global precipitation through perturbing the radiation budget. Studies demonstrated that global precipitation decreases in the next few years following large volcanic eruptions (Iles & Hegerl, 2014; Joseph & Zeng, 2011; Schneider et al., 2009; Trenberth & Dai, 2007). Decadal responses can also be excited by volcanic eruptions through internal feedback of the climate system (Pausata et al., 2015; Schneider et al., 2009), and large volcanic forcing is found to be necessary for explaining the origin and duration of Little-Ice-Age-like perturbations in model simulations (Slawinska & Robock, 2017). Although volcanic eruptions are found to cool down the globe and reduce global precipitation, a recent study showed that volcanic eruptions in the Southern Hemisphere can enhance the global monsoon precipitation in the Northern Hemisphere mainly through enhancing the circulation, that is, inducing the convergence over the Northern Hemispheric monsoon region (Liu et al., 2016). The asymmetric effect of volcanic aerosols may cause different meridional distributions of surface temperature change and thus result in different precipitation responses, which also needs to be studied.

To answer the aforementioned question on how global precipitation changes under different combinations of the three external forcings, we seek guidance from the last millennium simulations. In section 2, we introduce the model simulations and statistical methods we have used. In section 3, we present the low-frequency climate variability caused by the individual solar forcing, volcanic forcing, and GHG forcing. In section 4, we discuss the hydrological sensitivity and analyze the energy budget. The spatial distribution of global surface temperature and precipitation changes is discussed in section 5. In section 6, we investigate the Arctic amplification of temperature increase and the Intertropical Convergence Zone (ITCZ) amplification of precipitation decrease caused by these external forcings. Conclusions and discussion of this study are given in section 7.

## 2. Model Simulations and Statistical Methods

To examine the roles of these external forcings, three millennium sensitivity experiments are performed by using the Community Earth System Model version 1. A 2,000-year control run, the same as that done

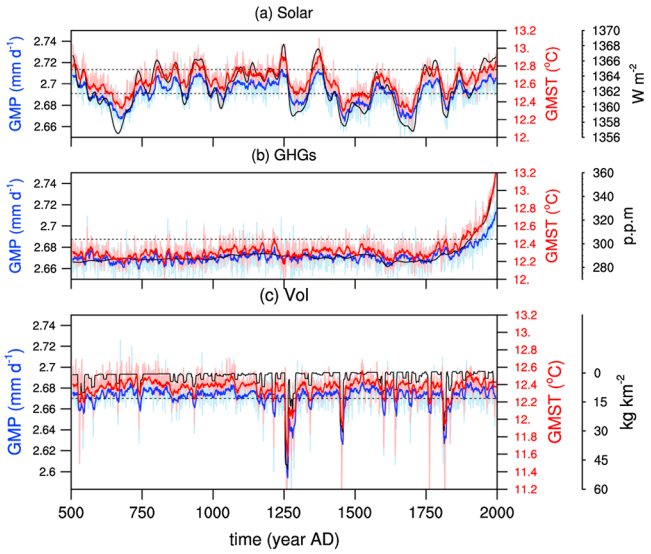


**Figure 1.** Individual external forcings and responses. Shown are the 11-year running mean time series of annual-mean external forcing (black curve) and simulated global mean surface temperature (GMST; thick red curve) and global mean precipitation (GMP; thick blue curve) under (a) solar forcing, (b) greenhouse gas (GHG) forcing, and (c) volcanic forcing. Simulated annual-mean values of GMST (thin red curve) and GMP (thin blue curve) are also shown as references. Note p.p.m. is parts per million.

by Rosenbloom et al. (2013) for the Paleoclimate Modeling Intercomparison Project Phase 3, is performed, in which the external forcing is fixed at the level of year 1850. Starting from this control run, three experiments with individual solar, volcanic, and GHG forcings are conducted for the period of 501 to 2000 CE. In these three experiments, the external forcing is the same as that in the control run, while the reconstruction of solar radiation (Shapiro et al., 2011), volcanic forcing (Gao et al., 2008), or GHG concentration (Macfarling Meure et al., 2006) is used as the only changing external forcing (Figure 1). The changes in the solar constant and the GHG concentration are globally uniform, while the aerosols of volcanic eruptions have meridional structures (Gao et al., 2008). In this work, the solar irradiance reconstruction of Shapiro et al. (2011) is used, thus leading to a large (0.5%) variation in the solar irradiance, which seems to be an overestimate of the likely actual variations (Judge et al., 2012; Jungclaus et al., 2017) and is far larger than that of the majority of more commonly used reconstructions (Schmidt et al., 2012). In some simulations, this high-amplitude reconstruction by Shapiro et al. (2011) causes a climate response incompatible with reconstructions (Feulner, 2011; Schurer, 2014), but this conclusion is model-dependent (Anet et al., 2014; Jungclaus et al., 2017). However, adoption of such a large forcing here is useful as it allows the effect of solar radiation to be clearly shown above the background internal variability.

For all these experiments, the resolution of T31 is used. The horizontal resolution is about 3.75° × 3.75° in the Community Atmosphere Model version 4, which is relatively coarse. For each forcing, only a single millennium run is performed. More details on model description can be found in Rosenbloom et al. (2013).

To reduce the strong interannual variability with a periodicity of 2–7 years, an 11-year running mean is applied for the model outputs. For these low-frequency time series, the effective degree of freedom should be considered while assessing significance. For two time series $x$ and $y$, the effective degrees of freedom $n_{\text{eff}}$ can be calculated by $n_{\text{eff}} = n/\left(1 + 2\sum_{i=1}^{n} r_{xt} r_{yt}\right)$, where $n$ is the number of samples and $r_{xt}$ and $r_{yt}$ are the autocorrelations at lag $t$ for these two time series (Liu et al., 2015; Livezey & Chen, 1983).

## 3. Low-Frequency Variability Induced by Different External Forcings

### 3.1. Simulated Low-Frequency Variability During the Last Millennium

Figure 1 shows the simulated global mean surface air temperature and precipitation under the individual forcing of solar radiation, volcanic eruptions, or GHGs. All three sensitivity experiments exhibit strong interannual variability of global mean surface temperature and precipitation, which is mainly caused by the internal modes. For the low-frequency variability in these 11-year-running-mean time series, the simulated global mean surface temperature variation agrees well with that of the simulated global mean precipitation, and their correlation reaches 0.98 for the solar experiment, 0.95 for the GHG experiment, and 0.96 for the volcanic experiment.

These simulated low-frequency variabilities also follow their external forcings closely. In the solar experiment (Figure 1a), a warm and wet period is simulated when solar radiation is strong, while a cold and dry period is caused by low solar radiation, especially the Little Ice Age from 1450 to 1850. This simulated low-frequency global mean surface temperature is also significantly correlated ($r = 0.94$, $p < 0.01$, and $n_{\text{eff}} = 22$) to the external solar radiation. In the GHG experiment (Figure 1b), the significant increases of global mean surface temperature and precipitation follow the increased GHG concentration well since the Industrial Revolution. Under global warming induced by the GHG forcing since 1850, the precipitation increase is much smaller than the temperature change, which is consistent with previous simulation results (Held & Soden, 2006;

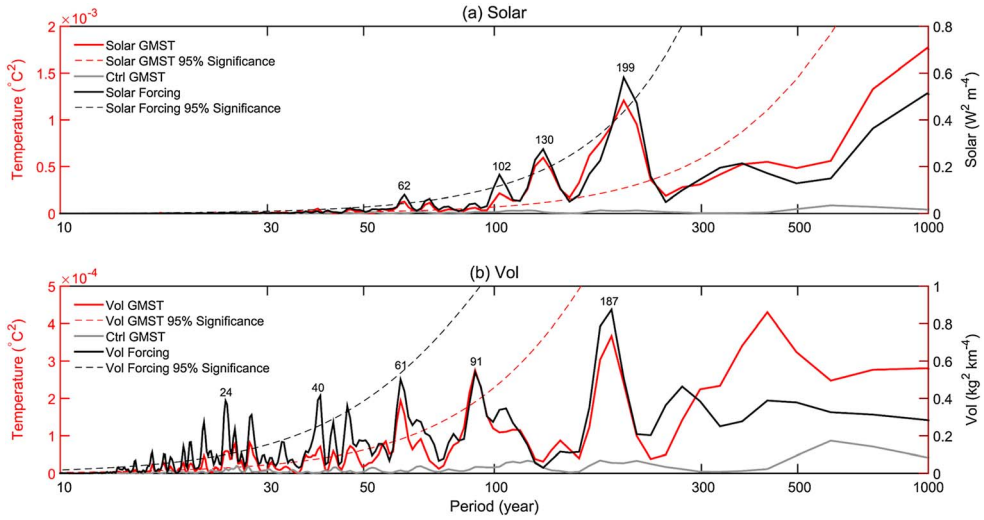


**Figure 2.** Power spectra of low-frequency variabilities of individual external forcings and responses. Shown are the power spectra of annual-mean external forcing (red line) and simulated global mean surface temperature (GMST; black line) under (a) solar forcing and (b) volcanic forcing. The spectrum of GMST in the control run (gray line) is also shown. Before spectral analysis, 11-year running mean is applied.

Liu et al., 2013). This is because the GHGs act as radiative absorbers to warm the troposphere, and the reduced tropospheric cooling should be balanced by less precipitation (Allen & Ingram, 2002).

In the volcanic experiment, the significant decreases of global mean surface temperature and precipitation are simulated in 2 years after explosive eruptions (Liu et al., 2016). For the low-frequency variation (Figure 1c), decreases of global mean surface temperature and precipitation are also simulated, and the correlation between the simulated global-mean surface temperature and volcanic aerosol concentration is $-0.84$ ($p < 0.01$, and $n_{\text{eff}} = 96$) for the period from 501 to 2000 CE. The negative correlation means that strong volcanic forcing should decrease the temperature. Strong long-term temperature and precipitation decreases are clearly shown after the 1257 Samalas volcano. This is consistent with previous work that suggests that the Samalas and the following three smaller eruptions in 1268, 1275, and 1284 might have triggered the Little Ice Age (Miller et al., 2012). As we know, stratospheric aerosols caused by a big eruption can only last for about 2 years (Robock, 2000), while both the collective effect of some successive eruptions and the internal feedback may contribute to this low-frequency response (Pausata et al., 2015; Schneider et al., 2009; Slawinska & Robock, 2017).

The power spectra of the 11-year running mean solar and volcanic forcings and their associated global mean temperature changes are shown in Figure 2, which are calculated by performing the Fourier transform on these time series. In both simulations, the interannual variability with a typical period of less than 10 years has been removed by the 11-year running mean, since the half-point of the response function for the 11-year running mean filter is around 22 years. In the solar experiment (Figure 2a), the global mean temperature coincides with the external forcing very well. The response and the volcanic forcing also agree with each other quite well (Figure 2b). Compared to the strong low-frequency variability in the solar and volcanic experiments, the low-frequency variability in the control run without any external forcing is very weak, which means that the low-frequency variability in the solar and volcanic experiments is caused by the solar or volcanic forcing.

Since the 11-year running mean can remove the strong interannual variability of the internal modes, the majority of the remaining low-frequency variation in these three sensitivity experiments is seen to be forced by the external forcing based on the following two conclusions: (1) the simulated low-frequency variation is highly correlated to the external forcing, with a correlation coefficient of 0.94, 0.84, and 0.94 in the solar, volcanic and GHG experiments, respectively; (2) the low-frequency variation in these three sensitivity experiments is much stronger than that in the control run without any changing external forcing, and the standard deviation of low-frequency global mean surface temperature is 0.13°C in the 1,500-year solar

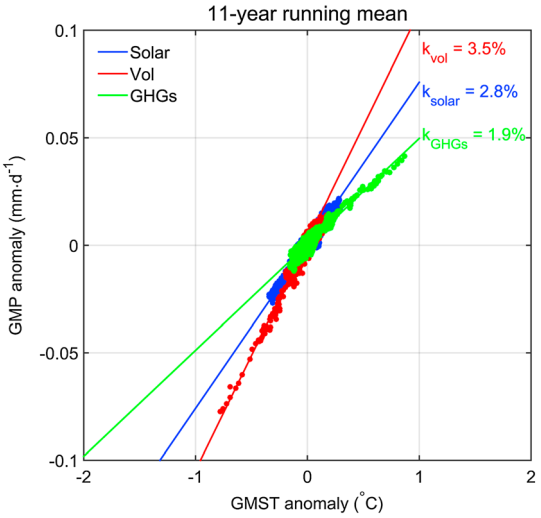


**Figure 3.** Scatterplot of low-frequency variabilities of global mean precipitation rate versus global mean surface temperature (GMST). Red, blue, and green dots show the 11-year running mean values of the annual-mean millennium simulations under individual volcanic, solar, and greenhouse gas (GHG) forcings, with regression slope of 3.4%/°C (0.094 mm day$^{-1}$ °C$^{-1}$), 2.8%/°C (0.076 mm d$^{-1}$ °C$^{-1}$), and 1.9%/°C (0.051 mm day$^{-1}$ °C$^{-1}$), respectively.

experiment, 0.11°C in the volcanic experiment, and 0.12°C in the GHG experiment, while it is only 0.04°C in the 2,000-year control run.

### 3.2. Definition of External Forcing-Induced Low-Frequency Changes

Since the low-frequency variability in these sensitivity experiments is excited or modulated by external forcing (Figures 1 and 2), responses to the solar forcing can be calculated by half of the difference between the composite of the 11-year running mean anomalies above one standard deviation and that below one negative standard deviation in the solar experiment (Figure 1a), responses to the GHG forcing can be calculated by the difference between the composite of the 11-year running mean anomalies above one standard deviation and the climatological mean in the GHG experiment (Figure 1b), and responses to the volcanic forcing can be calculated by the difference between the composite of 11-year running mean anomalies below minus one standard deviation and the climatological mean in the volcanic experiment (Figure 1c). With these criteria, the global warming induced by strong solar radiation is 0.2°C and that by large GHG concentration is 0.35°C, while the global cooling induced by strong volcanic eruption is −0.26°C. All these differences are significant at the 1% significance level using a two-sample *t*-test. In this work we focus on the hydrological sensitivity, and these amplitudes of global mean temperature change are only considered as references.

## 4. Hydrological Sensitivity and Energy Budget

### 4.1. Hydrological Sensitivity

Now we can calculate how much global precipitation will increase for a given temperature change induced by each external forcing. Figure 3 shows that global precipitation will increase 2.8% for a 1°C global temperature increase in the solar experiment, which is much larger than 1.9% in the GHG experiment. The change is 3.5% in the volcanic experiment, which is the largest among the three experiments. These results reveal that individual natural (solar or volcanic) forcing is more efficient in changing global precipitation than the anthropogenic forcing, which is consistent with previous simulations in other models (Andrews et al., 2010; Cao et al., 2012; Iles et al., 2013). For example, the ratios are 1.5%/°C for GHG forcing and 3.3%/°C for volcanic forcing in HadCM3 (Iles et al., 2013), which are 1.68%/°C for GHG forcing and 2.22%/°C for solar forcing in HadGEM1 (Andrews et al., 2010). Our results also show that the volcanic forcing is the most efficient external forcing in changing global precipitation. Keep in mind that we are comparing the efficiency in changing global precipitation on different timescales due to the natural variability of these three external forcings. The results may change when we use continuous volcanic aerosol forcing to perform the stratospheric aerosol modification in the Geoengineering Model Intercomparison Project.

### 4.2. Energy Budget

To understand these different hydrological sensitivities, the perturbation energy budget (Allen & Ingram, 2002; Mitchell et al., 1987) is applied here. For these low-frequency variations with radiative-convective equilibrium, global-mean precipitation must be balanced by evaporation. Following the analysis of Wu et al. (2013), the perturbation energy budget can be written as

$$L\Delta P = \Delta R_{LT} + \Delta R_{ST} + \Delta R_{LS} + \Delta R_{SS} + \Delta Q_S, \quad (1)$$

where $L = 2.5 \times 10^6$ J/kg is the latent heat of condensation and $P$ is the precipitation change. $R_{LT}$ and $R_{ST}$ are the net longwave and shortwave radiation change at the top of the atmosphere (TOA), respectively, and $R_{LS}$ and $R_{SS}$ are the net surface longwave and shortwave radiation change, respectively. $Q_s$ is the sensible heat flux change. $\Delta$ denotes the global average. In this work, the positive value denotes upward at the TOA and downward at the surface.

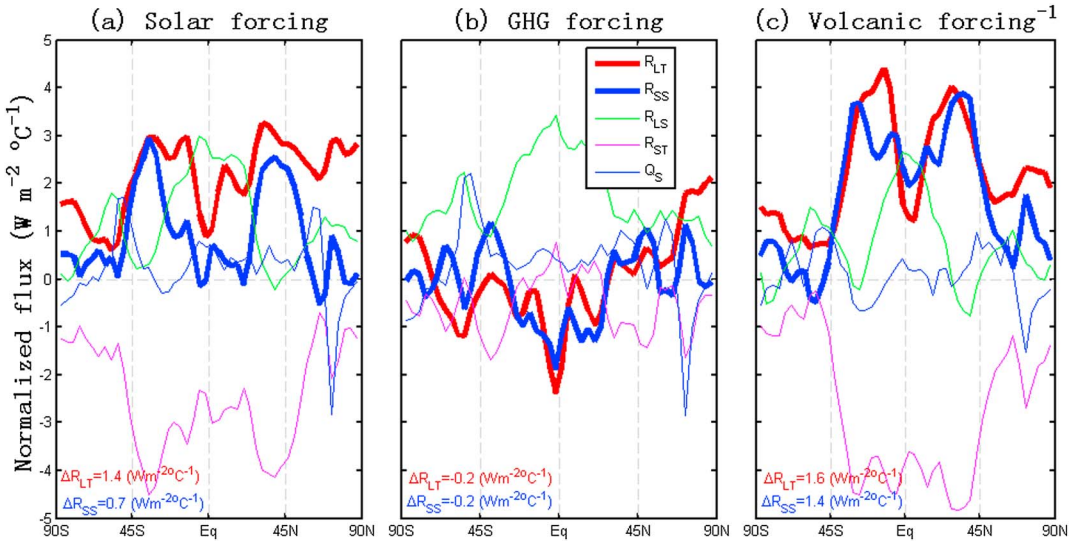


**Figure 4.** Global energy budget. Shown are zonal mean of low-frequency variabilities of normalized top of the atmosphere (TOA) net longwave (thick red line), surface net shortwave (thick blue line), surface net longwave (thin green line), TOA net shortwave (thin maroon line), and net sensible (thin blue line) heat fluxes under (a) solar forcing-induced global warming, (b) greenhouse gas forcing-induced global warming, and (c) volcanic forcing-induced global cooling. The positive value denotes upward at the top and downward at the surface. Each curve is normalized by its global mean temperature anomaly, and the anomaly in the volcanic experiment is multiplied by −1. The global-mean TOA net longwave and surface net shortwave radiation changes are also shown.

Figure 4 shows the changes in the fluxes of low-frequency variations forced by these external forcings. These low-frequency variations, which are defined in section 3, are divided by their respective global-mean surface temperature anomalies; thus, we can compare different responses to 1°C global-mean temperature change in the three experiments. Anomalies induced by the volcanic forcing are multiplied by −1. Results in the following figures are also normalized this way. The change of the total longwave radiation at the TOA is 1.4 W m$^{-2}$ °C$^{-1}$ in the solar experiment and 1.6 W m$^{-2}$ °C$^{-1}$ in the volcanic experiment. Both of them are upward. In the GHG experiment, however, this longwave radiation change is negative, that is, −0.2 W m$^{-2}$ °C$^{-1}$, and the maximum downward longwave radiation occurs near the equator (Figure 4b). This result means that increased GHG concentration will reduce the outgoing longwave radiation and weaken the tropospheric cooling; thus, its efficiency in changing precipitation is weaker than that of the solar and volcanic forcing, which is consistent with previous works (Andrews et al., 2010; Cao et al., 2012; Iles et al., 2013).

For global-mean surface temperature change of 1°Celsius, a big difference exists in the net surface shortwave radiation between the volcanic and solar experiments (Figures 4a and 4c). The global-average net shortwave radiation change at the surface is −1.4 W m$^{-2}$ °C$^{-1}$ under the volcanic forcing, which is twice that of the solar forcing. Such a large difference mainly occurs in the tropical regions. Compared to the solar forcing, the volcanic forcing causes strong solar irradiance change over the wet tropics, resulting in large precipitation change. These results call for a further investigation of the spatial distributions of these different responses.

## 5. Global Temperature and Precipitation Changes

The global surface temperature and precipitation changes induced by different external forcings are shown in Figure 5, in which the result of the volcanic simulation is reversed by multiplying −1 to compare with the results of the other two simulations. For strong solar radiation (Figures 5a and 5d), the westward gradient of SST is simulated over the equatorial Pacific, and the easterly wind anomalies are simulated over the central to eastern Pacific. Precipitation anomalies over the equatorial western Pacific are positive, while anomalies over the central to eastern Pacific are negative. Under the anthropogenic GHG forcing, the simulation shows an opposite result, which is represented by westerly wind anomalies over the eastern Pacific, positive precipitation anomalies over the equatorial central to eastern Pacific, and negative precipitation anomalies over the

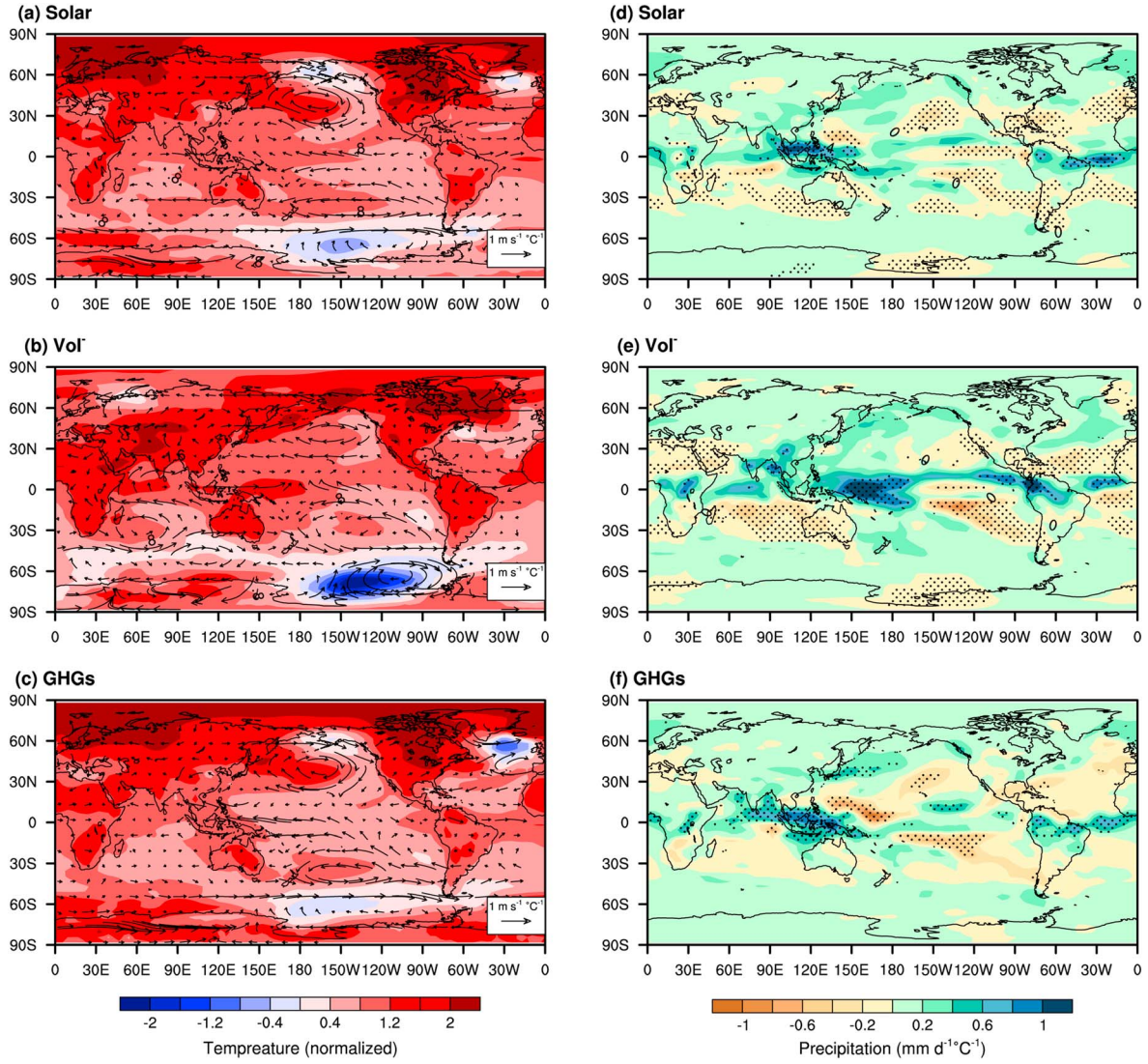


**Figure 5.** Spatial distributions of low-frequency temperature (left) and precipitation (right) changes induced by external forcings. Shown are the spatial patterns of low-frequency changes of annual-mean surface temperature (shading) induced by (a) solar, (b) volcanic, or (c) greenhouse gas (GHG) forcings, as well as the 850-hPa wind field (vector). Precipitation change under each forcing is also shown (d, e, and f). Each field is normalized by its global-mean temperature anomaly, and the anomaly in the volcanic experiment is multiplied by −1. Stippling indicates precipitation anomaly significant at the 5% significance level based on the *t* test. Most of the temperature changes are significant; thus, we do not show the significant test.

equatorial western Pacific (Figures 5c and 5f). The La Niña-like response under the solar forcing is similar with that simulated by the ECHO-G model (Liu et al., 2013). The eastern Pacific warming under the GHG forcing in our simulation is weaker than that in the ECHO-G model, while the precipitation response still resembles an El Niño type. The whole ITCZ is enhanced under weak volcanic forcing compared to that under strong volcanic forcing (Figure 5e). Next, we will examine the meridional distributions of the responses.

### 5.1. Meridional Temperature Change

The normalized zonally averaged surface temperature and precipitation anomalies induced by each external forcing are shown in Figure 6. Global warming is simulated with strong solar radiation and large GHG concentration, while global cooling is induced by large volcanic forcing (Figure 6a). For all three forcing fields, the global warming or cooling in the Northern Hemisphere is much larger than that in the Southern Hemisphere, and the midlatitude region of the Southern Hemisphere from 80°S to 50°S is the least affected region, which is associated with the cooling over the southern Pacific under the solar or GHG forcing and with

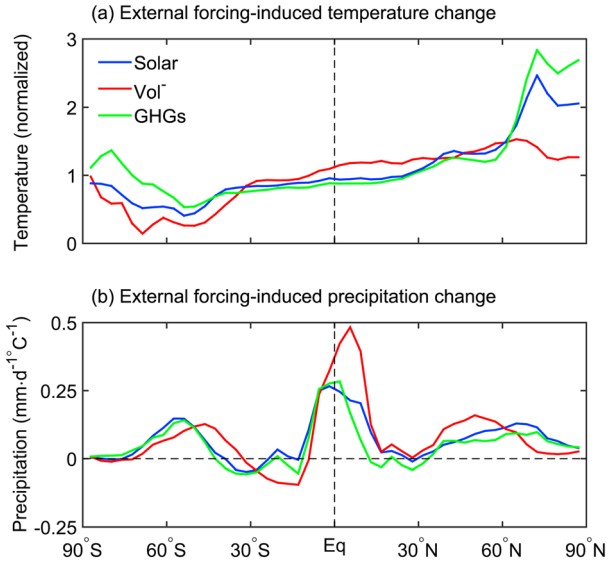


**Figure 6.** Meridional distributions of low-frequency temperature and precipitation change induced by external forcings. Shown are the zonal mean of low-frequency variabilities of annual-mean (a) surface temperature and (b) precipitation induced by solar (blue), volcanic (red), and greenhouse gas (GHG; green) forcings. Each curve is normalized by its global mean temperature anomaly, and the anomaly in the volcanic experiment is multiplied by −1.

the warming over the southern Pacific under the volcanic forcing (Figures 5a–5c). Under the volcanic forcing, strong warming is excited over the Southern Pacific (Figure 5b). It is caused by upwelling due to cyclonic wind anomalies that are teleconnected with tropical precipitation anomalies (Figure 5e). Thus, this strong oceanic warming tends to counteract the surrounding cooling, resulting in the weakest high-latitude temperature change over the Southern Hemisphere among the three external forcings (Figure 6a). Among these forcings, the low-latitude temperature change is also strongest for the volcanic forcing, because the latter induces strong solar irradiance change in the tropics (Figure 4). In this work the average of different volcanic events, that is, the tropical, Northern Hemispheric, and Southern Hemispheric eruptions, is used. For each type of eruptions, the meridional aerosol distribution and the associated radiation effect should be different.

Under global warming induced by solar radiation or GHG forcing, the largest warming occurs in the Arctic (Figure 6a), that is, the Arctic amplification. This is consistent with large upward sensible heat flux there (Figure 4). Arctic amplification has also been found in the past warming periods, as well as in historical observations and climate experiments (Barron, 1983; Bekryaev et al., 2010; Chapman & Walsh, 1993; Dahljensen et al., 1998; Holland & Bitz, 2003; Manabe & Wetherald, 1975). Divergent Arctic responses, however, are simulated in the three external forcing experiments. First, Arctic amplification induced by the GHG forcing is stronger than the results from the solar forcing. Second, Arctic amplification of temperature decrease does not exist in the volcanic experiment. Although high-latitude temperature decrease is below the global mean under the volcanic forcing, the maximum decrease occurs around 70°N and the Arctic temperature change is not that strong compared to the GHG or solar-induced change; thus, we still conclude that there is no Arctic amplification of temperature decrease in the volcanic experiment. Unlike volcanic aerosols, it is likely that anthropogenic aerosols have a large effect on the Arctic. Given that future projections of emissions of anthropogenic aerosols show a rapid reduction, this could lead to Arctic amplification (Navarro et al., 2016).

In summary, different north-south hemispheric asymmetric distributions of temperature change are induced by the three external forcings. For the 1°C global surface temperature change, the GHG forcing favors warming in the high-latitude regions and excites the strongest Arctic amplification among the three external forcing experiments. The volcanic forcing, however, excites the weakest high-latitude temperature change in both hemispheres, and no Arctic amplification of temperature decrease appears. Instead, the volcanic forcing causes the strongest low-latitude temperature change.

### 5.2. Meridional Precipitation Change

Strong solar radiation and large GHG concentration induce similar precipitation change, namely, large precipitation increase in the tropics and midlatitudes. The largest increase happens in the tropics (Figure 6b), which is consistent with the work of Meehl et al. (2007). Over the tropics and high latitudes of the Northern Hemisphere from 50°- to 70°N, precipitation increase induced by solar radiation is larger than that caused by the GHG forcing. Strong volcanic forcing induces a meridional distribution of precipitation change that has similar magnitude with but is opposite to those of the solar and GHG forcings, with large precipitation decrease appearing in the tropics and midlatitudes. Different from the nearly symmetric responses to solar radiation and GHG forcing, precipitation response to the volcanic forcing exhibits a strongly asymmetric structure, with the largest decrease occurring near 7°N. As shown in Figure 5e, this strong decrease is mainly caused by precipitation decrease of the ITCZ.

From Figure 6, we can conclude that among the solar, volcanic, and GHG forcings, the GHG forcing is the most efficient at causing Arctic amplification of temperature increase, while the volcanic forcing is the most efficient at inducing the ITCZ amplification of precipitation decrease. Now we also have an explanation for different efficiencies of external forcings in changing global precipitation. Compared with the solar

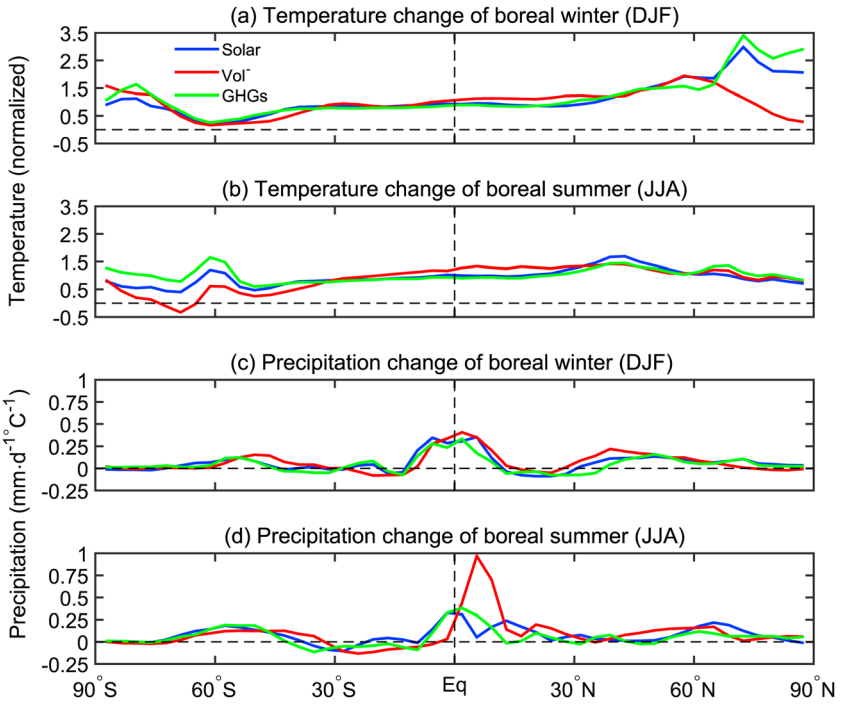


**Figure 7.** Season-dependent low-frequency temperature and precipitation change induced by external forcings. Same as Figure 6, except for the boreal winter (a, c) and boreal summer (b, d). JJA = June–August; DJF = December–February.

radiation, the GHG forcing is more efficient in causing high-latitude temperature increase and excites stronger Arctic amplification. Since high-latitude temperature change has a weak effect on precipitation change, solar radiation is more efficient at increasing global precipitation than the GHG forcing. Different from the GHG and solar forcings, which induce very strong high-latitude temperature change, the volcanic forcing tends to cause low-latitude temperature change, resulting in no Arctic amplification of temperature decrease but strong ITCZ amplification of precipitation decreases; thus, among the three external forcings, the volcanic forcing changes global precipitation most efficiently.

## 6. Arctic Amplification and ITCZ Amplification

Arctic and ITCZ amplifications are seasonally dependent (Figure 7). Arctic amplification under the GHG and solar forcings mainly occurs in the cold season of the Northern Hemisphere, that is, the boreal winter (Figure 7a). The high-latitude temperature change of the Southern Hemisphere also occurs in the cold season under the GHG forcing, while it is weak under the solar and volcanic forcings (Figure 7b). Large precipitation changes over the tropics and over the band of 30°–60° in both hemispheres are mainly found in boreal winter for all three external forcing fields (Figure 7c), while the ITCZ precipitation change induced by the volcanic forcing primarily occurs in boreal summer (Figure 7d).

The simulated strong winter Arctic amplification, associated with strong sea ice retreat under the anthropogenic GHG forcing (Figure 8a), is consistent with many previous works (Bintanja & Van Der Linden, 2013; Pithan & Mauritsen, 2014; Serreze et al., 2009; Serreze & Francis, 2006). During boreal summer, the Arctic obtains heat from the atmosphere mainly through downward shortwave and longwave radiation; in winter, the ocean releases heat into the atmosphere mainly through longwave radiation, sensible heat flux, and latent heat flux (Figure 8a), which is consistent with previous research (Bintanja & Van Der Linden, 2013).

Under the solar forcing, strong Arctic amplification also occurs in boreal winter (Figure 7a), when there is no solar radiation for the polar night. Seasonal transition of energy from summer to winter must be the reason (Figure 8b). During boreal summer, the Arctic obtains much heat from the atmosphere mainly via strong downward shortwave and longwave radiation. Heat obtained in the summer time is then released into the atmosphere to warm the air during boreal winter, which is associated with sea ice retreat. The upward

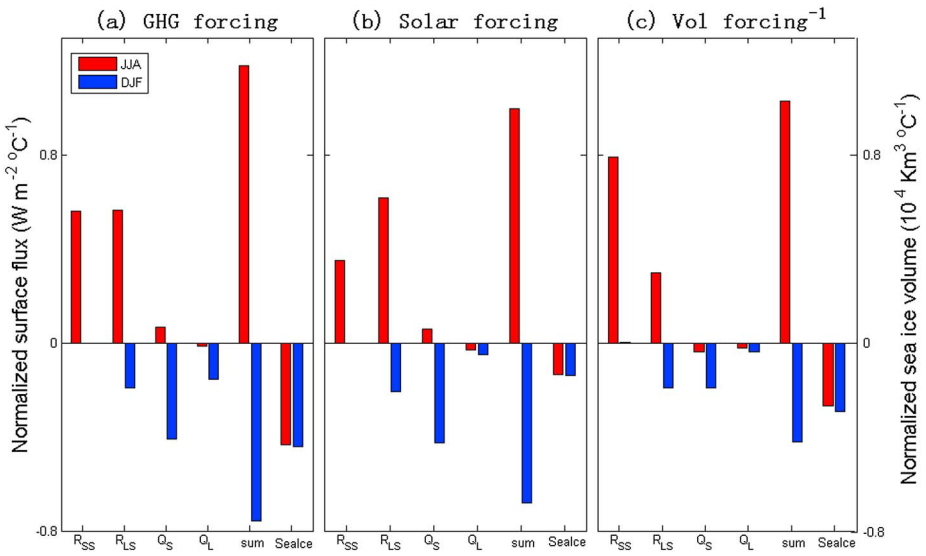


**Figure 8.** Seasonal Arctic surface energy balance and sea ice retreat. Shown are low-frequency variabilities of normalized Arctic (70–90°N average) net surface short wave radiation ($R_{SS}$), longwave radiation ($R_{LS}$), sensible heat flux ($Q_s$), latent heat flux ($Q_L$), their sum, and sea ice content for boreal summer (JJA, red) and winter (DJF, blue) under (a) greenhouse gas (GHG) forcing-induced global warming, (b) solar forcing-induced global warming, and (c) volcanic forcing-induced global cooling. The positive value denotes downward heat flux. Each value is normalized by its global mean temperature anomaly, and the anomaly in the volcanic experiment is multiplied by −1. JJA = June–August; DJF = December–February.

longwave radiation and strong sensible heat flux contribute to this strong winter heat release. Compared to the GHG experiment, the solar experiment witnesses relatively weaker summer heat obtainment and winter heat release, which result in weaker Arctic amplification.

Under the volcanic forcing, the Arctic loses a large amount of heat during boreal summer because of radiation reduction (Figure 8c). In comparison with the other two experiments, during boreal winter, heat transfer from the atmosphere to the ocean is relatively small, which explains why the winter Arctic amplification of temperature decrease is very weak under the volcanic forcing. Keep in mind that the results under the volcanic forcing are reversed by multiplying −1. Under strong volcanic forcing, Arctic sea ice content is strongly increased. This is consistent with previous work (Slawinska & Robock, 2017).

Compared to the other two experiments, why are the summer heat loss and sea ice content increase strong under the volcanic forcing? And why is the winter heat transfer to the ocean weak? One possible mechanism is the Atlantic poleward heat transfer associated with the Atlantic Meridional Overturning Circulation (AMOC). Our response to eruptions mainly stays on decadal to multidecadal timescale. On this timescale, CESM can simulate strong sea ice content increase and AMOC strengthening after explosive eruptions (Slawinska & Robock, 2017); thus, additional heat transfer from the tropics can warm the Arctic, resulting in small winter downward heat transfer from the atmosphere (Figure 8c). Further investigation of AMOC responses to different external forcings would be interesting but is beyond the scope of this paper.

ITCZ amplification of precipitation decrease induced by the volcanic forcing can be explained by the meridional distribution of volcanic aerosols. Because of frequent volcanic eruptions in the Northern Hemisphere (Liu et al., 2016), the amount of volcanic aerosols there is greater than that in the Southern Hemisphere; thus, the surface cooling induced in the Northern Hemisphere is stronger than its counterpart in the Southern Hemisphere (Figure 9a), resulting in strong northerly wind near the equator and divergence in the subtropics of the Northern Hemisphere (Figure 9b). The moisture decrease is also larger in the Northern Hemisphere than in the Southern Hemisphere (Figure 9b). The strong decrease of ITCZ precipitation is caused by both moisture decrease and circulation weakening (Figure 9c). This also explains why the Northern Hemispheric eruptions lead to the equatorward migration of the ITCZ (Colose et al., 2016; Pausata et al., 2015; Stevenson et al., 2016). Consistent with precipitation anomalies (Figure 7), this equatorward migration of the ITCZ mainly occurs during boreal summer (figure not shown).

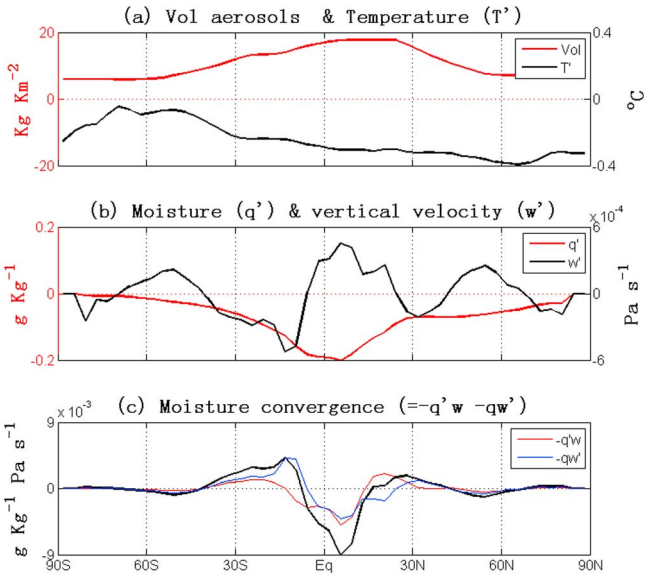


**Figure 9.** Asymmetry of volcanic forcing. Shown are the low-frequency variabilities of annual mean (a) volcanic forcing (red line) and zonal-mean temperature (dark line), (b) zonal-mean moisture (red line) and vertical velocity (black line), and (c) zonal-mean moisture convergence (black line) and moisture convergence induced by moisture anomaly (red line) and induced by circulation anomaly (blue line).

## 7. Concluding Remarks

By conducting three millennium sensitivity experiments using the Community Earth System Model version 1, the external solar, volcanic, and GHG forcing fields are found to excite different low-frequency variations in global mean surface temperature and precipitation (Figures 1 and 2). For a given amount of temperature change, GHG, solar, and volcanic forcing fields are revealed to have different efficiencies in changing global precipitation; the volcanic forcing is the most efficient one, followed by the solar forcing and GHG forcing (Figure 3). In view of global average, the reason is that the GHG forcing reduces tropospheric cooling and increases atmospheric stability, while the volcanic forcing induces the strongest solar irradiance change in the wet tropics (Figure 4). In regard to meridional asymmetry, the reason is that the GHG forcing causes more high-latitude warming in both hemispheres than the other forcing fields. It excites the strongest Arctic amplification of temperature increase in terms of global warming and favors changing temperature rather than increasing precipitation (Figure 6). Due to winter sea ice retreat, strong Arctic amplification occurs in winter under both GHG and solar forcings through the associated release of surplus ocean heat gained in summer (Figures 7 and 8). In terms of global cooling, the volcanic forcing cannot excite Arctic amplification of temperature decrease, though it causes the strongest low-latitude temperature change among these three forcings and results in strong boreal summer ITCZ amplification of precipitation decrease.

The effects of these different external forcings are summarized in Figure 10. The GHG forcing tends to reduce the outgoing longwave radiation, leading to weak precipitation increase (Figure 10a). Compared to the meridionally uniform solar forcing (Figure 10b), the volcanic forcing causes much stronger change in the solar irradiance over the wet tropics, resulting in stronger precipitation change (Figure 10c).

These new findings should provide us some new knowledge to tackle future volcanic eruptions or solar radiation variations under the anthropogenic GHG-induced global warming, thus enriching our understanding on the stratospheric aerosol modification method used to mitigate anthropogenic global warming (Crutzen, 2006; Pasztor et al., 2017). Potential volcanic eruptions have a limited effect against the GHG-induced global warming (Bethke et al., 2017), and it seems that the volcanic forcing or decrease of solar radiation cannot

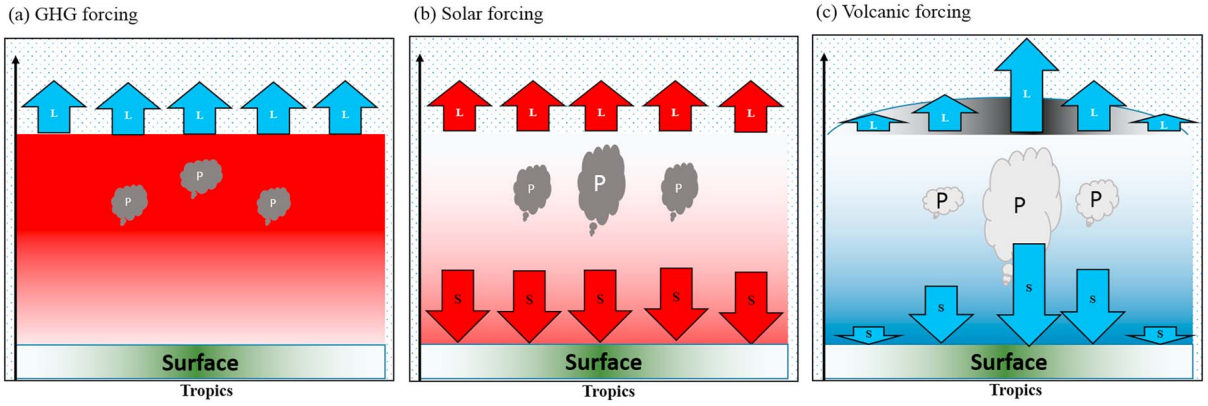


**Figure 10.** Different energy balances. Schematic diagram showing upward outgoing longwave radiation (L, upward vector), downward shortwave radiation (S, downward vector), as well as precipitation (cloud) anomalies under (a) GHG forcing and (b) solar forcing-induced global warming (red square), and (c) volcanic forcing-induced global cooling (blue square). The red/blue color denotes positive/negative anomaly, and positive/negative precipitation anomaly is denoted by the dark/gray color. The cloud size and vector length denote the strength of precipitation and radiation anomalies, respectively. The half ellipse denotes the volcanic aerosol concentration in the stratosphere.

mitigate the Arctic amplification induced by increased GHG concentration, even if they cause the same degree of temperature change. The finding obtained in this work is based on the coarse model resolution and one ensemble member from one model. Large intermodel spread of hydrological cycle has been found in different models (Fläschner et al., 2016; Pendergrass & Hartmann, 2012); thus, further analysis based on multimodel comparison should be conducted in the future.

**Acknowledgments**
This work was supported by the Natural Science Foundation of China (41420104002), the China National 973 Project (2015CB453200), the Natural Science Foundation of Jiangsu (BK20150907, 14KJA170002), the National Science Foundation of the US (AGS-1540783), and the Global Research Laboratory (GRL) Program of the National Research Foundation of Korea (2011-0021927). We thank two anonymous reviewers and one Associate Editor for thoughtful comments that have improved the manuscript. We also appreciate the helpful suggestions from Alan Robock that helped to improve the work. All reconstructions of the three external forcings are available at http://pmip3.lsce.ipsl.fr/. Simulation results are available at https://pan.baidu.com/s/1eRJvzl6 through password fpae. This paper is ESMC Contribution No. 209.

## References

Allen, M. R., & Ingram, W. J. (2002). Constraints on future changes in climate and the hydrologic cycle. *Nature*, *419*(6903), 224–232. https://doi.org/10.1038/nature01092

Andrews, T., Forster, P. M., Boucher, O., Bellouin, N., & Jones, A. (2010). Precipitation, radiative forcing and global temperature change. *Geophysical Research Letters*, *37*, L14701. https://doi.org/10.1029/2010GL043991

Anet, J. G., Muthers, S., Rozanov, E. V., Raible, C. C., Stenke, A., Shapiro, A. I., et al. (2014). Impact of solar versus volcanic activity variations on tropospheric temperatures and precipitation during the Dalton Minimum. *CliPa*, *10*(3), 921–938.

Barron, E. J. (1983). A warm, equable Cretaceous: The nature of the problem. *Earth Science Reviews*, *19*(4), 305–338. https://doi.org/10.1016/0012-8252(83)90001-6

Bekryaev, R. V., Polyakov, I. V., & Alexeev, V. A. (2010). Role of polar amplification in long-term surface air temperature variations and modern Arctic warming. *Journal of Climate*, *23*(14), 3888–3906. https://doi.org/10.1175/2010JCLI3297.1

Bethke, I., Outten, S., Ottera, O. H., Hawkins, E., Wagner, S., Sigl, M., & Thorne, P. (2017). Potential volcanic impacts on future climate variability. *Nature Climate Change*, *7*, 799–805.

Bintanja, R., Linden, E. C. V. D., & Hazeleger, W. (2012). Boundary layer stability and Arctic climate change: A feedback study using EC-Earth. *Climate Dynamics*, *39*(11), 2659–2673. https://doi.org/10.1007/s00382-011-1272-1

Bintanja, R., & Van Der Linden, E. (2013). The changing seasonal climate in the Arctic. *Scientific Reports*, *3*(1), 1556. https://doi.org/10.1038/srep01556

Cao, L., Bala, G., & Caldeira, K. (2012). Climate response to changes in atmospheric carbon dioxide and solar irradiance on the time scale of days to weeks. *Environmental Research Letters*, *7*(3), 034015. https://doi.org/10.1088/1748-9326/7/3/034015

Chapman, W. L., & Walsh, J. E. (1993). Recent variations of sea ice and air temperature in high latitudes. *Bulletin of the American Meteorological Society*, *74*(1), 33–47. https://doi.org/10.1175/1520-0477(1993)074%3C0033:RVOSIA%3E2.0.CO;2

Cobb, K. M., Charles, C. D., Cheng, H., & Edwards, R. L. (2003). El Nino/Southern Oscillation and tropical Pacific climate during the last millennium. *Nature*, *424*(6946), 271–276. https://doi.org/10.1038/nature01779

Colose, C. M., LeGrande, A. N., & Vuille, M. (2016). Hemispherically asymmetric volcanic forcing of tropical hydroclimate during the last millennium. *Earth System Dynamics*, *7*(3), 681–696.

Crutzen, P. J. (2006). Albedo enhancement by stratospheric sulfur injections: A contribution to resolve a policy dilemma? *Climatic Change*, *77*(3–4), 211–220. https://doi.org/10.1007/s10584-006-9101-y

Dahljensen, D., Mosegaard, K., Gundestrup, N., Clow, G. D., Johnsen, S. J., Hansen, A. W., & Balling, N. (1998). Past temperatures directly from the Greenland ice sheet. *Science*, *282*(5387), 268–271. https://doi.org/10.1126/science.282.5387.268

Feulner, G. (2011). Are the most recent estimates for Maunder Minimum solar irradiance in agreement with temperature reconstructions? *Geophysical Research Letters*, *38*, L16706. https://doi.org/10.1029/2011GL048529

Fläschner, D., Mauritsen, T., & Stevens, B. (2016). Understanding the Intermodel spread in global-mean hydrological sensitivity. *Journal of Climate*, *29*(2), 801–817.

Gao, C., Robock, A., & Ammann, C. (2008). Volcanic forcing of climate over the past 1500 years: An improved ice core-based index for climate models. *Journal of Geophysical Research*, *113*, D23111. https://doi.org/10.1029/2008JD010239

Haywood, J. M., Jones, A., Bellouin, N., & Stephenson, D. (2013). Asymmetric forcing from stratospheric aerosols impacts Sahelian rainfall. *Nature Climate Change*, *3*(7), 660–665. https://doi.org/10.1038/nclimate1857

Held, I. M., & Soden, B. J. (2006). Robust responses of the hydrological cycle to global warming. *Journal of Climate*, *19*(21), 5686–5699. https://doi.org/10.1175/JCLI3990.1

Holland, M. M., & Bitz, C. M. (2003). Polar amplification of climate change in coupled models. *Climate Dynamics*, *21*(3-4), 221–232. https://doi.org/10.1007/s00382-003-0332-6

Iles, C. E., & Hegerl, G. C. (2014). The global precipitation response to volcanic eruptions in the CMIP5 models. *Environmental Research Letters*, *9*(10), 104012. https://doi.org/10.1088/1748-9326/9/10/104012

Iles, C. E., Hegerl, G. C., Schurer, A. P., & Zhang, X. (2013). The effect of volcanic eruptions on global precipitation. *Journal of Geophysical Research: Atmospheres*, *118*, 8770–8786. https://doi.org/10.1002/jgrd.50678

Jones, A., Haywood, J. M., Alterskjær, K., Boucher, O., Cole, J. N. S., Curry, C. L., et al. (2013). The impact of abrupt suspension of solar radiation management (termination effect) in experiment G2 of the Geoengineering Model Intercomparison Project (GeoMIP). *Journal of Geophysical Research: Atmospheres*, *118*, 9743–9752. https://doi.org/10.1002/jgrd.50762

Joseph, R., & Zeng, N. (2011). Seasonally modulated tropical drought induced by volcanic aerosol. *Journal of Climate*, *24*(8), 2045–2060. https://doi.org/10.1175/2009JCLI3170.1

Judge, P. G., Lockwood, G. W., Radick, R. R., Henry, G. W., Shapiro, A. I., Schmutz, W., & Lindsey, C. (2012). Confronting a solar irradiance reconstruction with solar and stellar data. *Astronomy and Astrophysics*, *544*(3), 927–936.

Jungclaus, J. H., Bard, E., Baroni, M., Braconnot, P., Cao, J., Chini, L. P., et al. (2017). The PMIP4 contribution to CMIP6 – Part 3: The last millennium, scientific objective, and experimental design for the PMIP4 past 1000 simulations. *Geoscientific Model Development*, *10*(11), 4005–4033.

Kvalevåg, M. M., Samset, B. H., & Myhre, G. (2013). Hydrological sensitivity to greenhouse gases and aerosols in a global climate model. *Geophysical Research Letters*, *40*, 1432–1438. https://doi.org/10.1002/grl.50318

Liu, F., Chai, J., Huang, G., Liu, J., & Chen, Z. (2015). Modulation of decadal ENSO-like variation by effective solar radiation. *Dynamics of Atmospheres and Oceans*, *72*, 52–61. https://doi.org/10.1016/j.dynatmoce.2015.10.003

Liu, F., Chai, J., Wang, B., Liu, J., Zhang, X., & Wang, Z. (2016). Global monsoon precipitation responses to large volcanic eruptions. *Scientific Reports*, *6*(1), 24331. https://doi.org/10.1038/srep24331

Liu, J., Wang, B., Cane, M. A., Yim, S.-Y., & Lee, J.-Y. (2013). Divergent global precipitation changes induced by natural versus anthropogenic forcing. *Nature*, *493*(7434), 656–659. https://doi.org/10.1038/nature11784

Livezey, R. E., & Chen, W. (1983). Statistical field significance and its determination by Monte Carlo techniques. *Monthly Weather Review*, *111*(1), 46–59. https://doi.org/10.1175/1520-0493(1983)111%3C0046:SFSAID%3E2.0.CO;2

Macfarling Meure, C., Etheridge, D., Trudinger, C., Steele, P., Langenfelds, R., Van Ommen, T., et al. (2006). Law Dome $CO_2$, $CH_4$ and $N_2O$ ice core records extended to 2000 years BP. *Geophysical Research Letters*, *331*, L14810. https://doi.org/10.1029/2006GL026152

Manabe, S., & Wetherald, R. T. (1975). The effects of doubling the $CO_2$ concentration on the climate of a general circulation model. *Journal of the Atmospheric Sciences*, *32*(1), 3–15. https://doi.org/10.1175/1520-0469(1975)032%3C0003:TEODTC%3E2.0.CO;2

Mann, M. E., Cane, M. A., Zebiak, S. E., & Clement, A. (2005). Volcanic and solar forcing of the tropical Pacific over the past 1000 years. *Journal of Climate*, *18*(3), 447–456. https://doi.org/10.1175/JCLI-3276.1

Mann, M. E., Zhang, Z., Rutherford, S., Bradley, R. S., Hughes, M. K., Shindell, D., et al. (2009). Global signatures and dynamical origins of the Little Ice Age and Medieval Climate Anomaly. *Science*, *326*(5957), 1256–1260. https://doi.org/10.1126/science.1177303

Meehl, G. A., Stocker, T. F., Collins, W. D., Friedlingstein, P., Gaye, A. T., Gregory, J. M., et al. (2007). Global climate projections. In S. Solomon, et al. (Eds.), *Climate change 2007: The physical science basis. Contribution of Working Group I to the Fourth Assessment Report of the Intergovernmental Panel to Climate Change* (pp. 747–845). Cambridge, UK: Cambridge University Press.

Meehl, G. A., & Washington, W. M. (1996). El Niño-like climate change in a model with increased atmospheric $CO_2$ concentrations. *Nature*, *382*(6586), 56–60. https://doi.org/10.1038/382056a0

Miller, G. H., Geirsdóttir, Á., Zhong, Y., Larsen, D. J., Otto-Bliesner, B. L., Holland, M. M., et al. (2012). Abrupt onset of the lLittle Ice Age triggered by volcanism and sustained by sea-ice/ocean feedbacks. *Geophysical Research Letters*, *39*, L02708. https://doi.org/10.1029/2011GL050168

Mitchell, J. F. B., Wilson, C. A., & Cunnington, W. M. (1987). On $CO_2$ climate sensitivity and model dependence of results. *Quarterly Journal of the Royal Meteorological Society*, *113*(475), 293–322. https://doi.org/10.1256/smsqj.47516

Navarro, J. C. A., Ekman, A. M. L., Pausata, F. S. R., Lewinschal, A., Varma, V., Seland, Ø., et al. (2016). Future response of temperature and precipitation to reduced aerosol emissions as compared with increased greenhouse gas concentrations. *Journal of Climate*, *30*, 939–954.

Niemeier, U., Schmidt, H., Alterskjær, K., & Kristjánsson, J. E. (2013). Solar irradiance reduction via climate engineering: Impact of different techniques on the energy balance and the hydrological cycle. *Journal of Geophysical Research: Atmospheres*, *118*, 11,905–11,917. https://doi.org/10.1002/2013JD020445

Niemeier, U., & Tilmes, S. (2017). Sulfur injections for a cooler planet. *Science*, *357*(6348), 246–248. https://doi.org/10.1126/science.aan3317

O'Gorman, P. A., Allan, R. P., Byrne, M. P., & Previdi, M. (2012). Energetic constraints on precipitation under climate change. *Surveys in Geophysics*, *33*(3–4), 585–608. https://doi.org/10.1007/s10712-011-9159-6

Pasztor, J., Scharf, C., & Schmidt, K.-U. (2017). How to govern geoengineering? *Science*, *357*(6348), 231–231. https://doi.org/10.1126/science.aan6794

Pausata, F. S., Chafik, L., Caballero, R., & Battisti, D. S. (2015). Impacts of high-latitude volcanic eruptions on ENSO and AMOC. *Proceedings of the National Academy of Sciences of the United States of America*, *112*(45), 13,784–13,788. https://doi.org/10.1073/pnas.1509153112

Pendergrass, A. G., & Hartmann, D. L. (2012). Global-mean precipitation and black carbon in AR4 simulations. *Geophysical Research Letters*, *39*, L01703. https://doi.org/10.1029/2011GL050067

Pithan, F., & Mauritsen, T. (2014). Arctic amplification dominated by temperature feedbacks in contemporary climate models. *Nature Geoscience*, *7*(3), 181–184. https://doi.org/10.1038/ngeo2071

Planck, M. (1901). Ueber das Gesetz der Energieverteilung im Normalspectrum. *Ann Phys-berlin*, *309*(3), 553–563. https://doi.org/10.1002/andp.19013090310

Robock, A. (2000). Volcanic eruptions and climate. *Reviews of Geophysics*, *38*, 191–219. https://doi.org/10.1029/1998RG000054

Robock, A. (2016). Albedo enhancement by stratospheric sulfur injections: More research needed. *Earths Future*, *4*(12), 644–648.

Robock, A., Oman, L., & Stenchikov, G. L. (2008). Regional climate responses to geoengineering with tropical and Arctic $SO_2$ injections. *Journal of Geophysical Research*, *113*, D16101. https://doi.org/10.1029/2008JD010050

Rosenbloom, N., Otto-Bliesner, B., Brady, E., & Lawrence, P. (2013). Simulating the mid-Pliocene Warm Period with the CCSM4 model. *Geoscientific Model Development*, *6*(2), 549–561. https://doi.org/10.5194/gmd-6-549-2013

Schmidt, G. A., Jungclaus, J. H., Ammann, C. M., Bard, E., Braconnot, P., Crowley, T. J., et al. (2012). Climate forcing reconstructions for use in PMIP simulations of the last millennium (v1.0). *Geoscientific Model Development*, *4*(3), 1549–1586.

Schneider, D. P., Ammann, C. M., Otto-Bliesner, B. L., & Kaufman, D. S. (2009). Climate response to large, high-latitude and low-latitude volcanic eruptions in the Community Climate System Model. *Journal of Geophysical Research*, *114*, D15101. https://doi.org/10.1029/2008JD011222

Schurer, A. P. (2014). Small influence of solar variability on climate over the past millennium. *Nature Geoscience*, *7*(2), 104–108. https://doi.org/10.1038/ngeo2040

Screen, J. A., & Simmonds, I. (2010). The central role of diminishing sea ice in recent Arctic temperature amplification. *Nature*, *464*(7293), 1334–1337. https://doi.org/10.1038/nature09051

Serreze, M. C., Barrett, A. P., Stroeve, J. C., & Kindig, D. N. (2009). The emergence of surface-based Arctic amplification. *The Cryosphere*, *3*(1), 11–19. https://doi.org/10.5194/tc-3-11-2009

Serreze, M. C., & Francis, J. A. (2006). The Arctic amplification debate. *Climatic Change*, *76*(3–4), 241–264. https://doi.org/10.1007/s10584-005-9017-y

Shapiro, A. I., Schmutz, W., Rozanov, E., Schoell, M., Haberreiter, M., Shapiro, A. V., & Nyeki, S. (2011). A new approach to the long-term reconstruction of the solar irradiance leads to large historical solar forcing. *Astronomy and Astrophysics*, *529*(5), A69.

Slawinska, J., & Robock, A. (2017). Impact of volcanic eruptions on decadal to centennial fluctuations of Arctic Sea ice extent during the last millennium and on initiation of the Little Ice Age. *Journal of Climate*. https://doi.org/10.1175/JCLI-D-1116-0498.1171

Stevenson, S., Otto-Bliesner, B., Fasullo, J., & Brady, E. (2016). "El Niño like" hydroclimate responses to last millennium volcanic eruptions. *Journal of Climate*, *29*(8), 2907–2921. https://doi.org/10.1175/JCLI-D-15-0239.1

Trenberth, K. E., & Dai, A. (2007). Effects of Mount Pinatubo volcanic eruption on the hydrological cycle as an analog of geoengineering. *Geophysical Research Letters*, *34*, L15702. https://doi.org/10.1029/2007GL030524

Vecchi, G. A., Soden, B. J., Wittenberg, A. T., Held, I. M., Leetmaa, A., & Harrison, M. J. (2006). Weakening of tropical Pacific atmospheric circulation due to anthropogenic forcing. *Nature*, *441*(7089), 73–76. https://doi.org/10.1038/nature04744

Wu, P., Christidis, N., & Stott, P. (2013). Anthropogenic impact on Earth's hydrological cycle. *Nature Climate Change*, *3*(9), 807–810.

Zhang, L., & Li, T. (2014). A simple analytical model for understanding the formation of sea surface temperature patterns under global warming. *Journal of Climate*, *27*(22), 8413–8421. https://doi.org/10.1175/JCLI-D-14-00346.1